21st Australasian Fluid Mechanics Conference
Adelaide, Australia
10-13 December 2018

Structure of (Very) Rich n-dodecane Premixed Turbulent Flames at Diesel Engine Conditions: a Criterion to Distinguish Deflagrations from Autoignition Fronts

B. Savard[1], D. K. Dalakoti[1], A. Wehrfritz[1] and E. R. Hawkes[1,2]

[1]School of Mechanical and Manufacturing Engineering
University of New South Wales, Sydney, NSW 2052, Australia

[2]School of Photovoltaic and Renewable Energy Engineering
University of New South Wales, Sydney, NSW 2052, Australia

Abstract

In diesel flames, soot is produced in (very) rich mixtures (equivalence ratio up to approximately 5), downstream from a region of highly turbulent rich combustion. An important question that remains unanswered is whether combustion in this region consists of deflagrations (in which molecular diffusion plays an important role in assisting flame propagation), autoignition fronts (in which flame propagation is determined solely by chemical processses), or both, which is a roadblock to our current ability to predict the level of pollutants produced in diesel flames. In the present study, we address this fundamental question in a simplified, canonical configuration. Premixed turbulent deflagrations and autoignition fronts are studied in a statistically one-dimensional, doubly-periodic domain (which is instantaneously three-dimensional) using direct numerical simulations (DNS). The thermodynamic conditions are chosen to match those of the rich high-temperature burning region of Spray A, a target flame widely studied experimentally and numerically within the Engine Network Community (ECN). More specifically, the conditions are as follows: temperature of 732 K, pressure of 60 atm, and equivalence ratio of 3, with 15% vol. O_2 in the ambient gas. It is found that: 1) a transition from autoignition to deflagrations can be enabled by turbulence and 2) consistently, the flame structure of turbulent deflagrations is similar to that of laminar deflagrations, while that of turbulent autoignitions, resembles that of laminar autoignition fronts. These results suggest a simple criterion to distinguish turbulent deflagrations from turbulent autoignition fronts in the present rich flames.

Introduction

To coordinate diesel combustion research efforts towards a common goal, the Engine Combustion Network (ECN) [1, 17, 2, 14] has proposed a series of experimental reference flames at diesel engine conditions for model development and validation. Parametric variations of the Spray A case, an *n*-dodecane flame, have been extensively investigated [17, 2, 24, 3, 15, 14, 25].

Experimental and computational studies have revealed a highly complex flame structure, as summarized by Dec [6] and Musculus *et al.* [12]. Downstream of the liquid fuel spray, low-temperature chemistry (LTC) occurs first, a shrouding diffusion flame stabilizes in the products of LTC, a rich premixed combustion region sits in the center of the jet, inside the diffusion flame, and a sooting region follows downstream of the rich region. Previous studies have focused on aspects, such as the flame stabilization mechanism [18, 9], the ignition sequence [2, 24, 25], and soot formation [16, 13].

An aspect that has received little attention is the turbulence-chemistry interaction in the rich premixed combustion region, where the equivalence ratio can be at least five times larger than unity [13]. Both LTC and high-temperature chemistry (HTC) are involved in rich premixed diesel combustion [12]. In a very recent study [22], the authors addressed the problem of turbulence-chemistry interaction in this rich combustion mode by performing direct numerical simulations (DNS) of premixed turbulent flames at both thermochemical and turbulence conditions corresponding to Spray A. It was found that turbulence strongly affects the flame structure in physical space, with, for instance, a double-peaked reaction zone featuring simultaneously broken, thin, and distributed layers. In contrast, the flame structure in progress variable space matched very closely that of 1D laminar flames, thus suggesting the applicability of the flamelet tabulation approach to model rich premixed flames in Spray A. While it has not been fully established yet if combustion in this region occurs as a deflagration [6] or an autoignition front [12] (or both), as a first step, this previous study focused on rich premixed turbulent deflagrations.

Here, we extend the DNS study to investigate the transition between turbulent autoignition fronts and deflagrations. In particular, the objectives are to 1) analyze the transition in the absence of turbulence (1D laminar flames), 2) investigate the effect of turbulence on this transition, and 3) identify a criterion to distinguish turbulent autoignition fronts from turbulent deflagrations. In a separate paper, we apply the criterion established here to a downscaled DNS of Spray A.

Methodology

Numerical Approach

The numerical approach, described briefly, follows that of [20].

A statistically-planar, freely-propagating flame configuration was chosen in order to isolate the effects of turbulence on the flame from mean flow shear or curvature, such that direct comparison with an unstrained laminar reference flame is facilitated. A $12L \times L \times L$ rectangular prism domain is used with inflow/outflow in the x-direction and periodic boundary conditions in both the y- and z-directions. The unburnt gas is injected at constant bulk velocity with a low turbulent kinetic energy (TKE), such that there are no negative inlet velocities. Away from the inflow and outflow regions, velocity field forcing (described in [20]) maintains a constant TKE across the flame (more details on the turbulence statistics are given in [4]).

The low Mach number Navier-Stokes equations are solved numerically using the energy conserving, finite difference code NGA [7]. The selected scheme is second-order accurate in space and time. A semi-implicit Crank-Nicolson time integration is used [19, 23]. The third-order BQUICK scheme [8] is used for the scalar transport equations. NGA uses staggered, as opposed to collocated, operators, such that, at fixed order of accuracy, dispersive errors are significantly reduced [7].

A reduced 35-species *n*-dodecane mechanism [5] reduced from the Yao mechanism [26] is used, which contains high-

temperature and semi-global low-temperature chemistry pathways optimized for diesel engine conditions. Mixture-averaged diffusivities are used for species transport. Real gas effects are neglected. As shown by Lacaze *et al.* [11], under Spray A conditions, the compressibility factor is very close to unity (such that the ideal gas assumption is appropriate) for mixtures with equivalence ratio less than approximately 10.

The thermochemical conditions are selected to be representative of the rich combustion region in Spray A. An equivalence ratio of 3 is selected. The other conditions are set by considering adiabatic mixing between liquid *n*-dodecane fuel at 363 K and ambient gas at 900 K with 15% O_2 at a pressure of 60 atm (Spray A baseline case). As such, the temperature of the reactants is 732 K.

Reference Laminar Flames

Following the approach taken in [21], a series of 1D steady laminar flame simulations are performed over a range of inflow velocities (with the numerical solver described above). For high inflow velocities, conduction is negligible, such that chemical reactions are balanced by advection and the propagation regime consists of autoignition fronts. As inflow velocity is reduced, the contribution from conduction increases, up to a point from which heat and radicals are conducted upstream of the reaction zone, thus forming a preheat zone, characteristic of a deflagration, which sustains flame propagation. In this deflagration regime, as inflow velocity is further reduced, the flame attaches to the inlet (since the flame speed is larger than the inflow velocity) with heat loss occurring given the Dirichlet boundary condition considered. To identify the reference deflagration speed, S_L, the method of Krisman et al. [10] is used.

Figure 1 presents the heat release rate (HRR) structure in progress variable space ($c = Y_{H_2} + Y_{H_2O} + Y_{CO} + Y_{CO_2}$, with Y_i the mass fraction of species i) for inflow velocities spanning above and below S_L. It is clear that, as the flames transition from the autoignition regime to the deflagration regime, the HRR structure is significantly affected. In particular, a single-peak structure is found in the limit of 0D autoignition (or autoignition fronts with large inflow velocity) while deflagrations exhibit a double-peak structure.

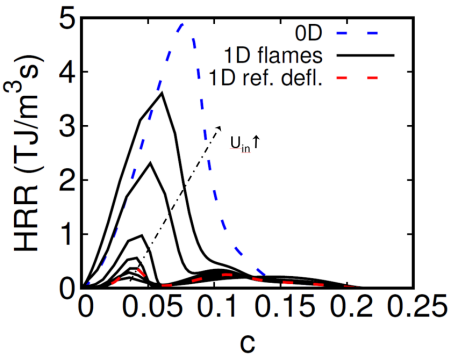

Figure 1: Heat release rate (HRR) vs. progress variable for 1D laminar flames with varying inflow velocities (U_{in}), ranging from 0.15 to 2.4 m/s and 0D ignition. The reference deflagration (red dashed line) corresponds to $U_{in} = S_L = 0.25$ m/s.

This transition is mainly a result of the reduction of HRR magnitude in the first peak, which is associated with LTC, rather than an increase in the second peak. Figure 2 shows the importance of LTC (represented here by the percentage of spatially integrated carbon flux through LTC) as a function of inflow velocity. It is observed that LTC is signifcantly more important in the limit of 0D ignition, with over three times more relative carbon flux through LTC than for deflagrations.

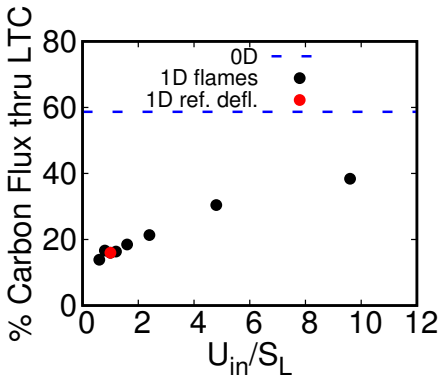

Figure 2: Percentage of spatially integrated carbon flux through LTC vs. inflow velocity.

While the present laminar flame results constitute a novel contribution, the aim for the rest of the paper is to assess if a similar transition in flame structure across the propagation regimes will be obtained in the presence of turbulence.

Turbulent Flames Simulation Parameters

The simulations are set up in order to span both the autoignition and deflagration regimes. In [21] it was found that at fixed inflow velocity, turbulence can trigger the transition from an initial laminar autoignition front to a deflagration. While only turbulent deflagrations where identified, it is expected that sufficiently high inflow velocity with sufficiently low turbulence can lead to a turbulent autoignition front. As such, here, turbulence intensity is varied to span the two regimes.

The turbulent flame parameters are listed in Table 1. The inflow velocity is fixed at 2.4 m/s, which corresponds to approximately 10 times S_L. The ratio of integral length scale to laminar flame thickness, l/l_F, is fixed to unity and the ratio of rms of velocity fluctuations, u'/S_L, is varied from 6 to 15. As such, the turbulent flames are nominally in the thin reaction zones regime. Note that a Karlovitz number of the order of 100 is expected in rich premixed flames in Spray A, based on the work of Pei et al. [15]. For all four cases, the flame is initialized with the

Case	A	B	C	D
u'/S_L	6	9	12	15
l/l_F		1.0		
Ka_u	40	70	110	160
$Re_{t,u}$	60	80	110	140
U_{in} (m/s)		2.4		

Table 1: Simulation parameters. $S_L = 0.25$ m/s and $l_F = 38\,\mu$m. $Ka_u = t_F/t_{\eta_u}$ is defined as the ratio of flame time $t_F = l_F/S_L$ to Kolmogorov time scale $t_{\eta_u} = \left(\nu_u l/u'^3\right)^{1/2}$, with ν_u the kinematic viscosity in the reactants. $Re_{t,u} = u'l/\nu_u$ and U_{in} is the bulk inflow velocity. The other parameters are defined in the text.

$U_{in} = 2.4$ m/s 1D laminar autoignition front, on which is superimposed a turbulent flow field, following the approach taken in [21] for cool flames.

Results and Discussion

Overview

Figure 3 presents 2D contours of RO_2 (LTC marker) and CH_2O (LTC product and HTC intermediate) mass fraction and HRR for flames A and D. In both cases, LTC, marked by RO_2 mass fraction, is clearly contained within the most upstream HRR region. While this region is spatially thin in Case A, it is strongly broken in Case D (similar structure observed in [22]).

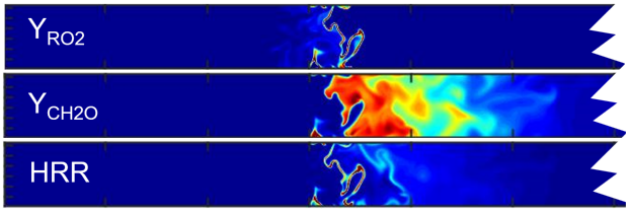

(a) Case A ($u'/S_L = 6$)

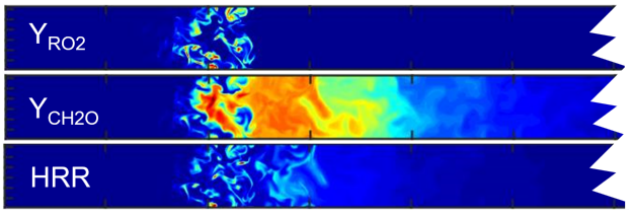

(b) Case D ($u'/S_L = 15$)

Figure 3: Contours of mass fraction of RO_2 (LTC marker) and formaldehyde (LTC product and HTC intermediate) and HRR on 2D slices. The inlet is on the left-hand-side and the domain has been cut on the right-hand-side for visualization purpose. The range for Y_{RO_2}, Y_{CH_2O}, and HRR are [0, 0.005], [0, 0.01], and [0, 1] TJ/m^{3}s, respectively. Red is maximum, blue is minimum.

Propagation Regime: Deflagration vs. Autoignition Front

Figure 4 presents the time evolution of the flame position, computed as

$$x_f(t) = 12L - \frac{1}{L^2 c_b}\int_\Omega c(x,y,z,t)\,\mathrm{d}V, \qquad (1)$$

where c_b is the value of the progress variable in the products. It can be observed that all flames initially move towards the inlet. However, flame A eventually stabilizes at a location near the initial laminar ignition front location. It can therefore be identified as a turbulent autoignition front. In contrast, flames C and D continuously move steadily towards the inlet, indicating that these two flames are deflagrations. Finally, flame B may not be clearly categorized based on Fig. 4 and may be at the transition between the two regimes. A longer simulation time (associated with proportionally large computational cost) would provide a definite answer.

Flame Structure with Regime Transition

Figure 5 presents the conditional mean of HRR and mass fractions of CH_2O and RO_2 in progress variable space, with a comparison to laminar deflagrations (both mixture-averaged transport and unity Lewis number included). First, cases B, C, and D all three have a mean structure that is very close to that of laminar deflagrations. Note that the better match with unity Lewis number deflagrations, as found in [22], has been argued to be due to turbulent diffusion which drives the turbulent Lewis

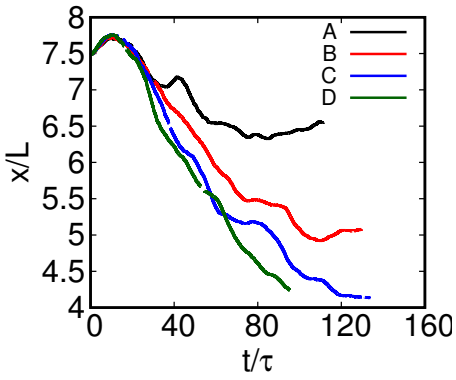

Figure 4: Flame position (normalized by the domain width) vs. time (normalized by the eddy turnover time u'/l for case D).

numbers towards unity. In contrast, consistent with the behavior in laminar flames (Fig. 1), Case A, which is a turbulent autoignition front, has a significantly larger first peak of HRR (in c space). This difference in flame structure, which is also apparent in the RO_2 mass fraction vs. c profiles, can serve as a criterion to distinguish turbulent autoignition fronts from turbulent deflagrations. Finally, we note that the contribution from LTC is significantly affected by turbulence, and following the transition towards the deflaragation regime observed in laminar flames, it is reduced from 38% (initial laminar flame) to approximately 20% (for all four cases).

Conclusions

DNS of rich turbulent *n*-dodecane premixed turbulent flames at diesel engine conditions were performed. The results of the present investigation indicate that: 1) increased turbulence enables the transition from autoignition to deflagrations and 2) consistently, the flame structure follows a similar transition, ranging from a laminar ignition front-like structure to a laminar deflagration-like structure under the effect of increased turbulence. This transition between these two distinct flame structures can be used as a criterion to distinguish turbulent deflagrations from turbulent autoignition fronts.

Acknowledgements

This work was supported by the Australian Research Council and computational resources from Pawsey, National Computational Infrastructure and Intersect awarded through the National Computational Merit Allocation Scheme, and the Academic Computer Center in Gdańsk (CI TASK).

References

[1] Engine Combustion Network, https://ecn.sandia.gov, 2017.

[2] Benajes, J., Payri, R., Bardi, M. and Martí-Aldaraví, P., Experimental characterization of diesel ignition and lift-off length using a single-hole ecn injector, *Appl. Therm. Eng.*, **58**, 2013, 554 – 563.

[3] Bhattacharjee, S. and Haworth, D. C., Simulations of transient n-heptane and n-dodecane spray flames under engine-relevant conditions using a transported pdf method, *Combust. Flame*, **160**, 2013, 2083 – 2102.

[4] Bobbitt, B., Lapointe, S. and Blanquart, G., Vorticity transformation in high karlovitz number premixed flames, *Phys. Fluids*, **28**, 2016, 015101.

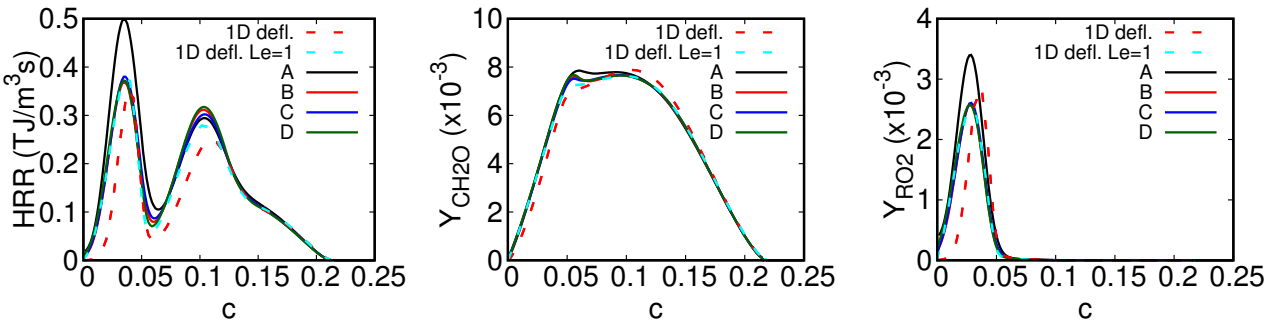

(a) (b) (c)

Figure 5: Conditional mean of HRR, Y_{RO_2}, and Y_{CH_2O} vs. progress variable. The profiles for mixture-averaged and unity Lewis number laminar deflagrations are included for comparison.

[5] Borghesi, G., Krisman, A., Lu, T. and Chen, J. H., Direct numerical simulation of a temporally evolving air/n-dodecane jet at low-temperature diesel-relevant conditions, *Combust. Flame*, **195**, 2018, 183–202.

[6] Dec, J. E., A conceptual model of di diesel combustion based on laser-sheet imaging*, *SAE Technical Paper*, 970873.

[7] Desjardins, O., Blanquart, G., Balarac, G. and Pitsch, H., High order conservative finite difference scheme for variable density low mach number turbulent flows, *J. Comput. Phys.*, **227**, 2008, 7125–7159.

[8] Herrmann, M., Blanquart, G. and Raman, V., Flux corrected finite volume scheme for preserving scalar boundedness in reacting large-eddy simulations, *AIAA Journal*, **44**, 2009, 2879–2886.

[9] Krisman, A., Hawkes, E. R. and Chen, J. H., Two stage autoignition and edge flames in a high pressure turbulent jet, *J. Fluid. Mech.*, **824**, 2017, 5–41.

[10] Krisman, A., Hawkes, E. R. and Chen, J. H., The structure and propagation of laminar flames under autoignitive conditions, *Combust. Flame*, **188**, 2018, 399–411.

[11] Lacaze, G., Misdariis, A., Ruiz, A. and Oefelein, J. C., Analysis of high-pressure Diesel fuel injection processes using LES with real-fluid thermodynamics and transport, *Proc. Comb. Inst.*, **35**, 2015, 1603–1611.

[12] Musculus, M. P. B., Miles, P. C. and Pickett, L. M., Conceptual models for partially premixed low-temperature diesel combustion, *Prog. Energy Combust. Sci.*, **39**, 2013, 246–283.

[13] Pandurangi, S. S., Bolla, M., Wright, Y. M., Boulouchos, K., Skeen, S. A., Manin, J. and Pickett, L. M., Onset and progression of soot in high-pressure n-dodecane sprays under diesel engine conditions, *Int. J. Engine Res.*, **18**, 2017, 5–6.

[14] Pei, Y., Davis, M. J., Pickett, L. M. and Som, S., Engine Combustion Network (ECN): Global sensitivity analysis of Spray A for different combustion vessels, *Combust. Flame*, **162**, 2015, 2337–2347.

[15] Pei, Y., Hawkes, E. R., Bolla, M., Kook, S., Goldin, G. M., Yang, Y., Pope, S. B. and Som, S., An analysis of the structure of an n-dodecane spray flame using TPDF modelling, *Combust. Flame*, **168**, 2015, 420–435.

[16] Pei, Y., Som, S., Pomraning, E., Senecal, P. K., Skeen, S. A., Manin, J. and Pickett, L. M., Large eddy simulation of a reacting spray flame with multiple realizations under compression ignition engine conditions, *Combust. Flame*, **162**, 2015, 4442–4455.

[17] Pickett, L. M., Genzale, C. L., Bruneaux, G., Malbec, L.-M., Hermant, L., Christiansen, C. and Schramm, J., Comparison of diesel spray combustion in different high-temperature, high-pressure facilities, *SAE Int. J. Engines*, **3**, 2010, 156–181.

[18] Pickett, L. M., Kook, S., Persson, H. and Andersson, O., Diesel fuel jet lift-off stabilization in the presence of laser-induced plasma ignition, *Proc. Comb. Inst.*, **32**, 2009, 2793–2800.

[19] Pierce, C. D., *Progress-variable approach for large-eddy simulation of turbulent combustion*, Ph.D. thesis, Stanford University, 2001.

[20] Savard, B., Bobbitt, B. and Blanquart, G., Structure of a high Karlovitz n-C_7H_{16} premixed turbulent flame, *Proc. Comb. Inst.*, **35**, 2015, 1377–1384.

[21] Savard, B., Wang, H., Teodorczyk, A. and Hawkes, E. R., Low-temperature chemistry in n-heptane/air premixed turbulent flames, *Combust. Flame*, **196**, 2018, 71–84.

[22] Savard, B., Wang, H., Wehrfritz, A. and Hawkes, E. R., Direct numerical simulations of rich premixed turbulent n-dodecane/air flames at diesel engine conditions, *Proc. Comb. Inst.*, in press.

[23] Savard, B., Xuan, Y., Bobbitt, B. and Blanquart, G., A computationally-efficient, semi-implicit, iterative method for the time-integration of reacting flows with stiff chemistry, *J. Comput. Phys.*, **295**, 2015, 740–769.

[24] Skeen, S. A., Manin, J. and Pickett, L. M., Simultaneous formaldehyde PLIF and high-speed schlieren imaging for ignition visualization in high-pressure spray flames, *Proc. Comb. Inst.*, **35**, 2015, 3167–3174.

[25] Wehrfritz, A., Kaario, O., Vuorinen, V. and Somers, B., Large Eddy Simulation of n-dodecane spray flames using Flamelet Generated Manifolds, *Combust. Flame*, **167**, 2016, 113–131.

[26] Yao, T., Pei, Y., Zhong, B.-J., Som, S., Lu, T. and Luo, K. H., A compact skeletal mechanism for n-dodecane with optimized semi-global low-temperature chemistry for diesel engine simulations, *Fuel*, **191**, 2017, 339–349.